

Few-Shot Fingerprinting

Subject Re-Identification in 3D-MRI and 2D-X-Ray

Gonçalo Gaspar Alves², Shekoufeh Gorgi Zadeh¹, Andreas Husch², Ben Bausch¹

¹University of Luxembourg ²Former Association with University of Luxembourg
ben.bausch@uni.lu

Abstract. Combining open-source datasets can introduce data leakage if the same subject appears in multiple sets, leading to inflated model performance. To address this, we explore subject fingerprinting, mapping all images of a subject to a distinct region in latent space, to enable subject re-identification via similarity matching. Using a ResNet-50 trained with triplet margin loss, we evaluate few-shot fingerprinting on 3D MRI and 2D X-ray data in both standard (20-way 1-shot) and challenging (1000-way 1-shot) scenarios. The model achieves high Mean-Recall-@-K scores: 99.10% (20-way 1-shot) and 90.06% (500-way 5-shot) on ChestXray-14; 99.20% (20-way 1-shot) and 98.86% (100-way 3-shot) on BraTS-2021.

1 Introduction

In our context, subject re-identification does not aim to reveal the subject’s identity from anonymized data, as described in [1], but identifying all images that belong to the same subject. Therefore we find the term subject fingerprinting more suitable. This technique leverages anatomical structures and pathophysiological conditions as unique markers to associate an image with a specific individual. This formulation is very useful in dataset aggregation, where we need to identify subjects present in multiple datasets in order to avoid data leakage.

Some methods for subject reidentification in MRI, such as [2], use majority voting comparing multiple 2D slices from a pair of 3D MRI volumes to detect duplicate or near-duplicate volumes. Similar to our work, [3] and [4] compare latent space embeddings of multiple images to determine if they belong to the same subject. To generate these image embeddings, researchers commonly apply deep neural networks to encode the images to fixed size embedding vectors. Training such models can be done in an unsupervised manner, as the only form of supervision needed is knowing which images belong to which subject. This information is inherently provided by the structure of the datasets. Many few-shot learning algorithms can be applied to this problem by considering the subjects to be classes with only a few samples.

1.1 Few-Shot Learning

Few-Shot Learning is a subfield of machine learning focused on extracting meaningful features from limited samples per class, useful in data-scarce domains such as medical imaging. Problems are typically framed as N -way K -shot tasks, where N denotes the

number of classes and K the number of samples per class. The main approaches include Transfer-Learning, Meta-Learning, and Metric-Learning. Transfer-Learning fine-tunes pre-trained models for new classes, Meta-Learning enables rapid adaptation from related tasks [5], and Metric-Learning optimizes distance metrics to cluster similar samples and separate dissimilar ones [1] [6]. This work adopts Metric-Learning for its simplicity and the absence of suitable $3D$ biomedical pre-trained models. The model minimizes Euclidean distances between embeddings of the same subject while maximizing distances between different subjects.

2 Materials and Methods

2.1 Models

In our experiments, we employ the $2D$ and $3D$ ResNet-50 [7] [8] architectures, two popular and efficient neural network architectures well-suited to our problem setting. ResNet-50 is a convolutional neural network that utilizes residual blocks to mitigate the vanishing gradient problem. We use the final output of the model as an embedding for subject fingerprinting.

2.2 Datasets

X-Ray: For the $2D$ X-ray fingerprinting task, we utilized the NIH Chest X-ray Dataset (also known as ChestXray-14), published as an extension of the ChestXray-8 dataset [9]. This large-scale dataset contains 112'120 frontal-view chest X-ray images from 30'805 unique subjects collected between the years 1992 and 2015. The images show a large variety of image quality, subject position and posture, and up to fourteen common thoracic pathologies, making image augmentations, beyond normalization and resizing to a 512 x 512 resolution, unnecessary. We use the train-validation-test split from [1].

BraTS2021: For the $3D$ MRI fingerprinting task, we utilized the Brain Tumor Segmentation (BraTS) 2021 dataset from the MICCAI BraTS Challenge [10], [11] and [12]. This multi-institutional dataset comprises 1'251 subjects with brain tumors, each providing magnetic resonance imaging (MRI) scans with multiple modalities. Due to the limited natural variance in brain shape and position across modalities, we applied affine transformations to the images during training and resized the images to 78 x 120 x 120. We randomly split the data on a patient-wise basis into a 70% – 10% – 20% train-validation-test split.

2.3 Training

At each iteration step, we randomly select subjects from the train split and uniformly sample two images per subject to create a batch of anchor images and a batch of positive images. Following the work on Siamese Neural Networks [13], we encode the anchors and the positives using the same learnable model parameters. For each anchor-positive tuple, we search for an appropriate negative sample among the anchor images of distinct subjects within the batch. Finally, we use the triplet margin loss [6], defined in *Equation*

I, to train the model by comparing the anchor embeddings, the positive and the negative samples.

2.4 Triplet Margin Loss

The triplet margin loss aims at minimizing the distance between the associated anchor a and positive embedding p , pulling together the embeddings of the images of the same subject. However, relying only on this pulling force would lead to a model collapse. Therefore, we need an additional pushing force that maximizes the dissimilarity of embeddings coming from images of different subjects. To establish this, the triplet margin loss relies on a negative sample n and maximizes the distance between the anchor and negative embeddings. The triplet margin loss encourages the distance between the anchor and a hard negative to be larger than the distance between the anchor and a positive by at least margin α . A hard negative sample per anchor-positive tuple is selected from the batch of anchors. The triplet margin loss [14] is given as:

$$\mathcal{L}_{trip}(a, p, n) = \max(d(a, p) - d(a, n) + \alpha, 0) \quad (1)$$

Selecting random negatives from the batch is usually not enough for the network to learn meaningful embeddings. Negatives that are highly dissimilar to the anchor are easy-negatives and lead to a loss value of 0. Therefore, we employ an in-batch mining strategy [14], as described in *Algorithm 1*, to find hard negatives in the batch for each anchor-positive tuple. Due to this mining strategy, it is crucial that the batch size is large enough to include suitable hard negatives for the anchor-positive tuples.

2.5 Evaluation and Metrics

We evaluate the models using an N -way K -shot framework, where N represents the number of distinct subjects and K denotes the number of support images available for each subject. For each subject, we assess the retrieval metric based on a single query image q , aiming to retrieve all its corresponding K support images. This means that for each of the N queries, we retrieve the subjects top K most similar support images as a list $S_K = [s_1, \dots, s_K]$ ordered by the decreasing similarity scores.

The Recall-@- K ($Re_\varphi @ K$) measures the percentage of relevant images that have been retrieved across all N queries in the N -way K -shot problem φ . It is the ratio of query-relevant images retrieved, TP_q , to the total amount of relevant images $FN_q + TP_q = K$ averaged across all queries N .

$$Re_\varphi @ K = \frac{1}{N} \sum_{q=1}^N \frac{TP_q}{TP_q + FN_q} = \frac{1}{N} \sum_{q=1}^N \frac{\sum_s^{S_K} rel(s, q)}{K} \quad (2)$$

where,

$$rel(s, q) = \begin{cases} 1 & s = subject_q \\ 0 & \text{else} \end{cases}$$

Alg. 1 Batched Hard Triplet Mining

Require: Anchors a , Positives p , SubjectIDs id , Distance Function d

```

1:  $n \leftarrow [\ ]$                                      ▷ Negative indices
2:  $bs = \text{length}(a)$                            ▷ Batch Size
3: for  $i = 1$  to  $bs$  do
4:    $d^+ = d(a_i, p_i)$                            ▷ Positive distance
5:    $\mathcal{T}_{hard} \leftarrow \emptyset$ 
6:   for  $j = 1$  to  $bs$  do
7:     if  $id_i \neq id_j$  then                      ▷ Validate subjects to be different
8:        $d^- = d(a_i, a_j)$                          ▷ Negative Distance
9:       if  $d^- \leq d^+$  then
10:         $\mathcal{T}_{hard}.\text{add}(a_j)$                   ▷ Hard Negative
11:       end if
12:     end if
13:   end for
14:   if  $\mathcal{T}_{hard} \neq \emptyset$  then                ▷ Random Hard Negative
15:      $n.\text{append}(\text{random}(\mathcal{T}_{hard}))$ 
16:   else
17:      $a.\text{remove}(a_i)$                            ▷ No Suitable Negative Found
18:      $p.\text{remove}(p_i)$ 
19:   end if
20: end for
21: return  $(a, p, n)$ 

```

In our setting, the number of retrieved images ($TP_q + FP_q = K$) equals the number of relevant images ($TP_q + FN_q = K$), therefore the Recall at K equals Precision at K .

Hit-@-R ($H_\varphi @ R$) is an additional metric that checks if at least a single relevant image has been retrieved within the R most similar ranking images. It indicates how well relevant images rank compared to non-relevant images.

$$H_\varphi @ R = \frac{1}{N} \sum_{q=1}^N \left(\bigvee_s^{S_R} \text{rel}(s, q) \right) \quad (3)$$

We repeat this experiment 100 times with N randomly sampled subjects and uniformly sample K supports and one query. Finally, we average the metrics across runs.

$$MRe@K = \frac{1}{100} \sum_{\varphi=1}^{100} \text{Recall}_\varphi @ K \quad \text{and} \quad MH@R = \frac{1}{100} \sum_{\varphi=1}^{100} H_\varphi @ R \quad (4)$$

To assess embedding cluster quality, we calculate Mean Intra-Subject Distance (MIASD) and Mean Inter-Subject Distance (MIESD) as shown in *Figure 2 (A)*. MIASD measures how closely a subject's embeddings cluster around their mean embedding. MIESD measures the average distance between different subjects' mean embeddings. Together, these metrics reveal within-cluster tightness and between-cluster separation.

3 Results

<i>N</i> -way - <i>K</i> -shot	<i>MRe@K</i>			<i>MH@1</i>			<i>MH@5</i>		
	SSIM	Pack	Ours	SSIM	Pack	Ours	SSIM	Pack	Ours
20-1	30.95	99.25	99.10	30.95	99.25	99.10	59.20	99.65	100.0
20-5	27.24	99.57	98.24	49.55	99.85	99.70	73.05	99.90	99.95
100-1	17.96	99.24	97.46	17.96	99.24	97.46	32.85	99.53	99.58
100-5	15.91	99.20	95.33	33.05	99.81	99.17	51.12	99.86	99.72
500-1	11.19	98.80	94.60	11.19	98.80	94.60	19.31	99.33	98.66
500-5	9.82	98.55	90.06	23.03	99.66	98.05	35.25	99.53	99.44
1000-1	9.55	98.51	92.30	9.55	98.51	92.30	16.08	99.18	97.95

Tab. 1. ChestXray-14: SSIM, Pack and our performance on the test dataset across different *N*-way *K*-shot settings.

<i>N</i> -way - <i>K</i> -shot	<i>MRe@K</i>			<i>MH@1</i>	<i>MH@3</i>
	20-1	99.20	99.20	99.65	
20-3	99.25	99.72	99.78		
100-1	98.86	98.86	99.25		
100-3	98.79	99.44	99.53		

Tab. 2. BraTS-2021: our ResNet-50 performance on the test dataset across different *N*-way *K*-shot settings.

On the ChestXray-14 dataset, we compared the retrieval performances of our method to two other approaches (Table 1): **SSIM** [15], a well-established similarity measure, is used to compare pairs of images. The images are downsampled to 256x256 resolution due to the slow nature of comparing images on a pixel basis. Similar to our method, [4] (**PACK**) compares the image embeddings of a ResNet-50 and is trained using a margin-based contrastive loss, however, they additionally make use of cross-batch memory [16]. In Table 1, we can observe that for all models the *MRe@K* performance drops as the amount of subjects increase, as it is more likely to include images from other subjects that are similar to the query images. On the other hand, the 5-shot settings show better *MH@1* and *MH@5* scores as more images from the same subject in the set of all possible images increase the possibility to include an image that is more similar to the query. Similarly, on the BraTS-2021 dataset, our method achieves a high performance on all metrics and the scores slightly decay with increasingly harder test settings. On ChestXray-14, Pack consistent outperforms our method, which we conclude to originate from two main differences: Pack is trained on higher resolution images (1024x1024) also used during retrieval. Using cross-batch memory, Pack can keep more negative samples in memory increasing the amount of good anchor-negative pairs during training.

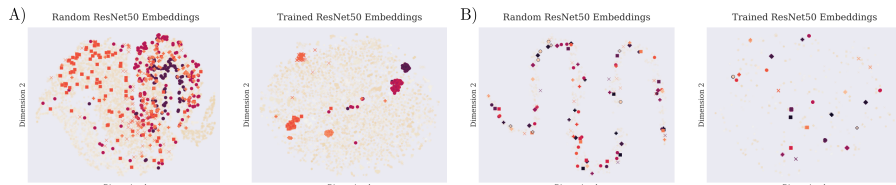


Fig. 1. T-SNE plots of 128-dimensional image embeddings from the ChestXray-14 (A) and the BraTS-2021 (B) test sets, highlighting a selection of subjects. (A & B left) Untrained ResNet-50 encodings, showing no clustering of subjects. (A & B right) ResNet-50 trained with triplet margin loss, showing clustered and well-separated subjects in latent space.

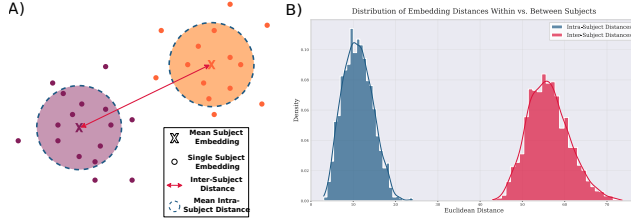


Fig. 2. (A) Abstraction of the MIASD and MIESD. B) Binned Intra-Subject (Blue) and Inter-Subject Distances (Red) for all subjects in the ChestXray-14 dataset.

In *Figure 1*, we qualitatively show the models' ability to generate embeddings that form distinct clusters for images of the same subject within the latent space and effectively separate different subjects on the BraTS-2021 and ChestXray-14 datasets. In *Figure 2 (B)*, we quantitatively assess the clustering performance of the models using the MIESD and MIASD metrics. On ChestXray-14, the model achieved a MIASD value of 11.08 ± 4.96 , and a MIESD value of 56.17 ± 3.46 . On BraTS-2021, the model generates embeddings with a MIASD value of 3.01 ± 1.97 and a MIESD value of 52.03 ± 8.17 . This shows a clear separation of distinct subjects while clustering the images of the same subject in latent space.

4 Discussion

In conclusion, our simple training strategy demonstrates to be highly capable of differentiating and fingerprinting both 2D and 3D medical subject images. However, these results could be further improved by adding strategies circumventing memory limitations, such as cross-batch memory for contrastive learning. To the best of our knowledge, this is the first work using 3D volumetric biomedical data as input to a model for subject fingerprinting, and performing cross-modal MRI subject retrieval. We show that images from the same subject cluster together, while clusters of different subjects are well separated. This identification mechanism makes our approach particularly valuable for detecting near-duplicate images in both 2D and 3D medical image datasets, thereby providing a novel approach to mitigate data leakage when aggregating datasets in clinical research and machine learning applications.

5 Code and Data

The code can be found in the following repository <https://github.com/BenBausch/Few-Shot-Fingerprinting> and the data can be downloaded under the following links: NIH Chest X-rays <https://www.kaggle.com/datasets/nih-chest-xrays/data> and BraTS2021 <https://www.kaggle.com/datasets/dschettler8845/brats-2021-task1/data>.

6 Acknowledgments

The results presented in this article were obtained using the HPC facilities of the University of Luxembourg [17] (<https://hpc.uni.lu>).

References

1. Packhäuser K, Gündel S, Münster N, Syben C, Christlein V, Maier A. Deep learning-based patient re-identification is able to exploit the biometric nature of medical chest X-ray data. *Scientific Reports*. 2022;12(1):14851.
2. Truong T, Jush FK, Lenga M. Benchmarking Pretrained Vision Embeddings for Near- and Duplicate Detection in Medical Images. 2024 IEEE International Symposium on Biomedical Imaging (ISBI). 2024:1–5.
3. Macpherson MS, Hutchinson CE, Horst C, Goh V, Montana G. Patient reidentification from chest radiographs: an interpretable deep metric learning approach and its applications. *Radiology: Artificial Intelligence*. 2023;5(6):e230019.
4. Packhäuser K, Gündel S, Münster N, Syben C, Christlein V, Maier A. Deep learning-based patient re-identification is able to exploit the biometric nature of medical chest X-ray data. *Scientific Reports*. 2022;12(1).
5. Finn C, Abbeel P, Levine S. Model-agnostic meta-learning for fast adaptation of deep networks. *International conference on machine learning*. PMLR. 2017:1126–35.
6. Vassileios Balntas Edgar Riba DP, Mikolajczyk K. Learning local feature descriptors with triplets and shallow convolutional neural networks. *Proceedings of the British Machine Vision Conference (BMVC)*. Ed. by Richard C. Wilson ERH, Smith WAP. BMVA Press, 2016:119.1–119.11.
7. He K, Zhang X, Ren S, Sun J. Deep Residual Learning for Image Recognition. *CoRR*. 2015;abs/1512.03385.
8. Hara K, Kataoka H, Satoh Y. Learning spatio-temporal features with 3d residual networks for action recognition. *Proceedings of the IEEE international conference on computer vision workshops*. 2017:3154–60.
9. Wang X, Peng Y, Lu L, Lu Z, Bagheri M, Summers R. ChestX-ray8: Hospital-scale Chest X-ray Database and Benchmarks on Weakly-Supervised Classification and Localization of Common Thorax Diseases. 2017 IEEE Conference on Computer Vision and Pattern Recognition (CVPR). 2017:3462–71.
10. Baid U, Ghodasara S, Bilello M, Mohan S, Calabrese E, Colak E et al. The RSNA-ASNR-MICCAI BraTS 2021 Benchmark on Brain Tumor Segmentation and Radiogenomic Classification. *CoRR*. 2021;abs/2107.02314.
11. Menze BH, Jakab A, Bauer S, Kalpathy-Cramer J, Farahani K, Kirby J et al. The multimodal brain tumor image segmentation benchmark (BRATS). *IEEE transactions on medical imaging*. 2014;34(10):1993–2024.
12. Bakas S, Akbari H, Sotiras A, Bilello M, Rozycki M, Kirby JS et al. Advancing the cancer genome atlas glioma MRI collections with expert segmentation labels and radiomic features. *Scientific data*. 2017;4(1):1–13.
13. Bromley J, Guyon I, LeCun Y, Säckinger E, Shah R. Signature verification using a "siamese" time delay neural network. *Advances in neural information processing systems*. 1993;6.
14. Schroff F, Kalenichenko D, Philbin J. Facenet: A unified embedding for face recognition and clustering. *Proceedings of the IEEE conference on computer vision and pattern recognition*. 2015:815–23.
15. Nilsson J, Akenine-Möller T. Understanding SSIM. 2020.
16. Wang X, Zhang H, Huang W, Scott MR. Cross-Batch Memory for Embedding Learning. *CoRR*. 2019;abs/1912.06798.
17. Varrette S, Cartiaux H, Peter S, Kieffer E, Valette T, Olloh A. Management of an academic HPC & research computing facility: The ULHPC experience 2.0. *Proceedings of the 2022 6th High Performance Computing and Cluster Technologies Conference*. 2022:14–24.